OPTICAL CHARACTERIZATION BY ELLIPSOMETRY - A PROSPECTIVE

D.E. Aspnes

Bell Laboratories, Murray Hill, New Jersey 07974, U.S.A.

Résumé - Les caractéristiques suivantes rendent l'éllipsométrie utile pour résoudre de nombreux problèmes concernant les corps solides, les interfaces et les couches minces : sensibilité aux monocouches et microstructures, précision intrinsèque, grande résolution en énergie et possibilité d'effectuer des mesures sur des corps transparents. Cet article est consacré aux problèmes posés par les déviations par rapport aux échantillons parfaits : théorie du champ moyen, théorèmes sur les limites, méthodes pour déterminer avec précision les spectres de la fonction dielectrique de corps solides réels et de couches minces, et effets de la texture microscopique sur les spectres. On donne des exemples de caractérisation *in situ* pendant le décapage, le nettoyage, la croissance et le dépôt de couches minces, et on discute les relations entre l'éllipsométrie spectroscopique et les autres méthodes de caractérisation.

Abstract - Submonolayer and microstructural sensitivity, intrinsic accuracy, high energy resolution, and the capability of obtaining data in any transparent ambient make ellipsometry a useful technique for addressing a number of problems in solids, interfaces, and thin films. This paper covers topics concerned with deviations from sample perfection: effective medium theory, limit theorems, methods of obtaining accurate dielectric function spectra on real bulk and thin film samples, and the effects of microstructure on these spectra. Examples of in situ characterization of etching, cleaning, growth, and sample deposition are given, and the relation of spectroscopic ellipsometry to other characterization methods is discussed.

I. INTRODUCTION

The vigorous development of photometric designs /1/ in the last decade has added a spectroscopic dimension to ellipsometry while retaining the usual advantages of submonolayer sensitivity and the capability of making nondestructive measurements in any transparent ambient. The instrumentation problems in the visible-near uv spectral range have largely been solved, and interest has shifted to the quantitative interpretation of dielectric response spectra, analysis of materials and interfaces, and other practical applications. Today one need no longer work with nearly ideal samples; meaningful measurements can be made on bulk or thin-film specimens that may be anisotropic, inhomogeneous, microscopically rough, covered with adsorbed layers, or have finite interface widths.

Optical characterization requires accurate data, or more precisely, accurate spectral data. This is the province of spectroscopic ellipsometry (SE), and most of the paper will deal with SE and the type of information that we can learn from the dielectric function ($\epsilon = \epsilon_1 + i\epsilon_2$) data obtainable with automatic spectroscopic instruments. Length limitations require compromises, so I shall assume that topics associated with ideal samples -- the propagation of electromagnetic radiation in homogeneous media, reflection at mathematically sharp boundaries, n-phase models -- are familiar since they are thoroughly discussed elsewhere /2/. I shall concentrate on topics designed to deal with deviations from sample perfection: effective medium theory, limit theorems, methods of obtaining accurate ϵ spectra of real samples, and the effects of microstructure on ϵ spectra. Examples include sample cleaning and film deposition, where such deviations are the norm. The reader interested in further details and applications is directed to previous reviews by J. Theeten and me /3,4/, to a previous review of ellipsometry by Neal /5/, and to a series of articles on optical methods of thin film analysis in two recent issues of Acta Electronica /6/.

II. BASIC PRINCIPLES -- INSTRUMENTATION

An ellipsometer determines the complex reflectance ratio, $\rho = r_p/r_s$, of a reflecting sample, where r_p and r_s are the complex reflectances of p- and s-polarized light, respectively. The older null designs obtained ρ by establishing polarization states that extinguished the flux reaching the detector. The quadratic dependence of the intensity on instrument settings near null and the necessity of operating the detector at very low light levels limited null ellipsometers

to very intense spectral line sources. SE is dominated by photometric instruments, where one of the elements is rotated or otherwise modulated to systematically vary the flux reaching the detector /1/. In addition to being readily automated, photometric instruments operate at high optical efficiency and are ideally suited for use with the weak continuum sources of optical spectroscopy.

The approximately 30 groups that have built or are building their own SEs have cast their economic ballots almost exclusively for three configuration. These are the rotating analyzer, rotating polarizer, and phase modulated ellipsometers, or RAE, RPE, and PME for short. The RAE and RPE have certain advantages of simplicity because the only wavelength-dependent element is the sample itself. Systematic errors are less likely with a RAE than with a RPE because polarization-insensitive detectors are available while polarization-free sources are not. However, a RAE cannot be used if the sample or its environment are themselves appreciable sources of light. The PME is not affected by source polarization or detector polarization sensitivity, is capable of high-speed operation, has no mechanically moving parts, and is a true Stokes polarimeter that can distinguish circular from unpolarized light. However, the modulation amplitude of the dynamic compensator is another free parameter that must be varied with wavelength and which should be measured independently. The invention of a truly achromatic compensator would make both RAE and RPE configurations instantly obsolete, since a rotating-compensator ellipsometer would eliminate the major disadvantages of both while losing none of the advantages.

III. BASIC PRINCIPLES -- THEORY

A. Dielectric Response

Much present optical characterization work concerns heterogeneous materials, where on a sufficiently fine length scale the dielectric function is itself a function of position. Unfortunately, the standard solutions of Maxwell's equations for homogeneous media provide no insight into this problem, and more fundamental approach is necessary. The key to understanding the optical properties of heterogeneous materials is to recognize that ϵ for any material must be calculated via a two-step process. An externally applied electric field causes displacements $\Delta\vec{r}_i$ of discrete charges q_i or charge densities $\rho(\vec{r})$. These screening charges give rise to corrections to the field on a microscopic scale. The first step is to solve this local-field problem self-consistently for the microscopic field $\vec{e}(\vec{r})$ and polarization $\vec{p}(\vec{r}) = \rho(\vec{r})\Delta\vec{r}$ at every point in space. But because the wavelength of light, λ, is far greater than the microstructural dimensions, only the macroscopic averages $\vec{E} = \langle\vec{e}(\vec{r})\rangle$ and $\vec{P} = \langle\vec{p}(\vec{r})\rangle$ can actually be observed. Consequently, the second step is to calculate these averages. If the material is isotropic, then ϵ is given by

$$\vec{D} = \epsilon\vec{E} = \vec{E} + 4\pi\vec{P} \qquad (1a,b)$$

where $\vec{D} = \langle\vec{d}(\vec{r})\rangle = \langle\vec{e}(\vec{r}) + 4\pi\vec{p}(\vec{r})\rangle$ is the macroscopic displacement field. For a set of discrete charges in a volume V, Eqs. (1) become

$$\vec{D} = \epsilon\vec{E} = \vec{E} + \frac{4\pi}{V}\sum_i q_i\Delta\vec{r}_i. \qquad (2a,b)$$

In Eqs. (2) displacements clearly depend on the bonding properties and the local fields, while the averaging process is represented by the sum and volume normalization. The normalization suggests that optical measurements can be a contactless means of determining sample density.

Thus, ϵ is a macroscopic average quantity. Whether a dielectric description makes sense depends on whether the averaging process itself makes sense. In some situations, as for example submonolayer distributions of adsorbed atoms on a substrate, a formulation in terms of atomic polarizabilities may be more realistic. The solve-average procedure is routine in many areas of physics, e.g., in quantum mechanics, but because classical electrodynamics -- like classical thermodynamics -- seeks to describe extremely complicated systems in terms of a few macroscopic observables, the microscopic origin of these equations is often forgotten.

B. Effective Medium Theory

Effective medium theory (EMT) allows the dielectric response of a heterogeneous material to be described by the dielectric functions of its constituents and a few wavelength-independent parameters and consequently is a basic tool in material characterization by optical means. If the separate regions are small compared to the wavelength of light but large enough to retain their own dielectric identity, the local-field problem can be solved by electrostatics. This quasistatic approximation describes many common and important situations.

The derivation of an EMT expression begins with a model microstructure. For example, we suppose a microstructure where all boundaries are parallel to the applied field. Then $\vec{e}(\vec{r}) = \vec{E}$ is everywhere constant and the spatial average over $\vec{d}(\vec{r})$ reduces simply to a spatial average over $\epsilon(\vec{r})$. For a two-phase composite this leads to

$$\epsilon = f_a\epsilon_a + f_b\epsilon_b,\ f_a + f_b = 1, \qquad (3a,b)$$

where ϵ_a and ϵ_b are the dielectric functions of the constituents and f_a and f_b are the respective volume fractions. If all boundaries are perpendicular to $\vec{E}$, then $\vec{d}(\vec{r}) = \vec{D}$ is everywhere constant and the spatial average over $\vec{\epsilon}(\vec{r})$ becomes

$$\epsilon^{-1} = f_a/\epsilon_a + f_b/\epsilon_b, \; f_a + f_b = 1. \qquad (4a,b)$$

All EMTs in the quasistatic approximation can be represented by /4/

$$\epsilon = \frac{q\epsilon_a\epsilon_b + (1-q)\epsilon_h(f_a\epsilon_a+f_b\epsilon_b)}{(1-q)\epsilon_h + q(f_a\epsilon_b+f_b\epsilon_a)}, \qquad (5)$$

where $0 \leqslant q \leqslant 1$ is a screening parameter and ϵ_h is the dielectric function of the background or "host" material. The standard Lorentz-Lorenz and Maxwell Garnett (MG) expressions and the Bruggeman effective medium approximation (EMA) are obtained for $q = 1/3$ (spherical microstructure) and $\epsilon_h = 1$, $\epsilon_h = \epsilon_a$ or ϵ_b and $\epsilon_h = \epsilon$, respectively, and thus differ only in the choice of host medium. There is no "universal" EMT for the same reason that there is no "universal" microstructure. Cermet (coated sphere) geometries are more accurately described by MG or symmetrized MG /7/ theories, while aggregates (collections of random particle shapes) are more accurately described by the EMA. The EMA shows a percolation threshold whereas MG does not. Under certain conditions the MG theory shows resonances which do not appear in the EMA. We have found the EMA to be generally applicable to thin films /4/, but there are many examples in the literature of bulk composites that are more accurately described by EMTs of the MG type /8,9/.

C. Limit Theorems

Given that there is almost complete freedom to choose any composition or microstructure, it is not at all obvious that the quasistatic approximation places well-defined limits on ϵ. But consider the simple cases discussed above. Equation (3) was derived by assuming that all internal boundaries were parallel to the applied field. In this case, no screening charge is developed. Since there can never be less screening than no screening, Eq. (3) must represent one limit to possible values of ϵ for a two-phase composite. Similarly, the maximum-screening situation occurs if all boundaries are perpendicular to the applied field. Since there can never be more screening than maximum screening, Eq. (4) must represent the other limit. Thus for any composition or microstructure, all values of ϵ calculated in quasistatic approximation must lie between the boundaries defined by Eqs. (3) and (4). These limits were established by Wiener in 1912 /10/ and are represented in Eq. (5) by $q = 0$ and $q = 1$, respectively.

More restrictive limits have also been derived. The Hashin-Shtrikman theorem /11/ defines the limits on ϵ if f_a is known. Then ϵ must lie within the region defined by the MG limits $\epsilon_h = \epsilon_a$ and $\epsilon_h = \epsilon_b$ for $0 \leqslant q \leqslant 1$ regardless of microstructure. The Bergman-Milton theorem /12,13/ defines the limits if in addition the sample is known to be isotropic to two ($q = 1/2$) or three ($q = 1/3$) dimensions. The Bergman-Milton limits are obtained simply by placing the Wiener bounds on ϵ_h. Because all limits can be expressed as bilinear transformations in the complex plane, all are easily constructed circular arcs /12/. An example for mixtures of hypothetical materials with $\epsilon_a = -2 + i3$ and $\epsilon_b = 1 + i1$ is given in Fig. 1.

The limit theorems provide guidelines as to what can and cannot be determined. They greatly simplify the entire EMT problem since all EMTs must conform to them /14/. They show further that composition is the more important variable if ϵ_a and ϵ_b are similar, while microstructure dominates if they are widely different. Also, while a detailed knowledge of the microstructure of a composite is an admirable objective, an exact solution would be about as useful as knowing the motions of the individual molecules in a macroscopic sample of a gas. It is far more important to be able to summarize the full complexity of a heterogeneous material in a few simple parameters via an EMT and to use the limit theorems to assess the reliability of these parameters. It should be obvious that a spectroscopic capability is essential in dealing with this problem /15/.

D. Finite Wavelength Effects

If the microstructural dimensions, d, are comparable to the wavelength, λ, scattering becomes important and the quasistatic approximation breaks down. However, it is still possible to define an effective dielectric function in terms of the wavevector for forward propagation of light /16/. The laminar microstructures giving the absolute Wiener bounds can also be solved exactly for any d/λ, giving some insight into the relative importance of this ratio /17/. Results for the special case discussed above are also shown in Fig. 1. The Wiener bounds are no longer rigorously valid, but the error is small for $d/\lambda \lesssim 0.1$. As d/λ increases, ϵ moves toward the value corresponding to that of the optically more dense medium due to a waveguiding phenomenon. In random composites the effects are more complicated, but the waveguiding interpretation seems to be a good first approximation /18/. The finite-wavelength solutions show that it is impossible for the macroscopic electromagnetic wave to conform to microstructural dimensions, so propagation takes place in an average sense.

E. Microscopic Roughness

A very important and very general manifestation of inhomogeneity occurs as microscopic roughness at sample surfaces. The eye tends to judge surface quality by macroscopic defects, but optically resolvable artifacts are generally not important in ellipsometry because they scatter light out of the field of the instrument. However, if the scale of irregularities is much less than λ, then the electromagnetic wave will neither scatter nor conform, and the surface region must be represented as an effective medium consisting of part substrate material and part ambient /15/.

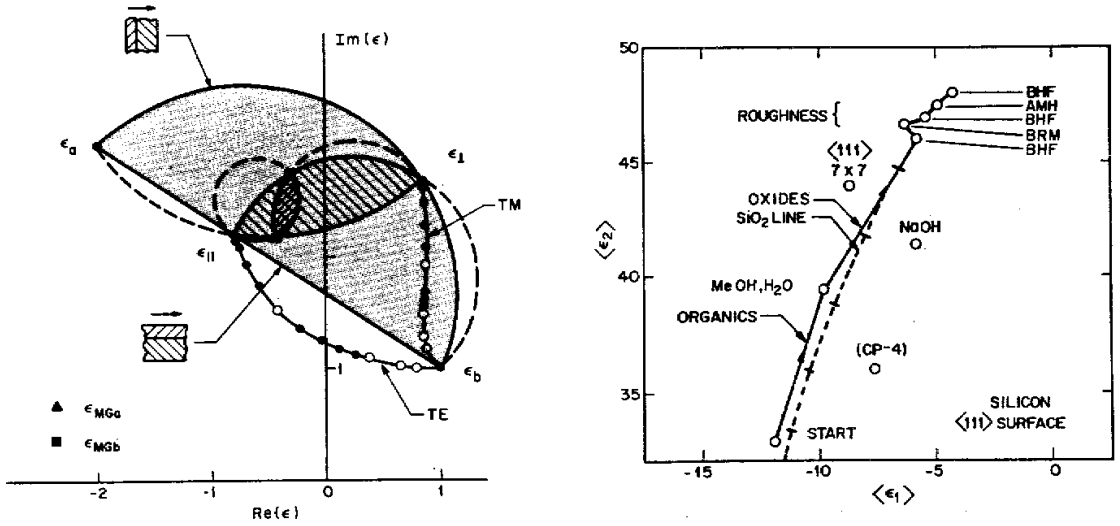

Fig. 1 Limits on ε for a composite with $\epsilon_a = -2 + i3$ and $\epsilon_b = 1 + i1$; for $f_a = 0.6$; for an isotropic sample with $q = 1/3$; for finite d/λ. In the finite-wavelength case the TE and TM modes correspond to propagation with the electric field parallel and perpendicular, respectively, to the laminations. The closed and open circles represent increments of 0.1 and 0.5, respectively, in d/λ.

Fig. 2 Removal of an air-grown natural overlayer on a c-Si wafer measured at 4.24 eV. Results of other treatments are also shown.

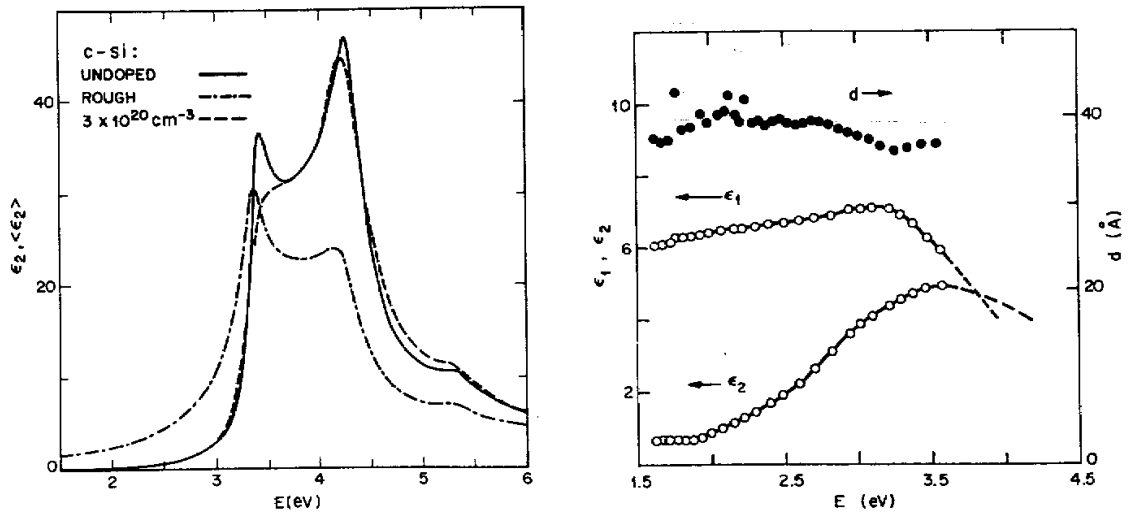

Fig. 3 Representative SE spectra for c-Si: ϵ_2, undoped; c-Si: $\langle\epsilon_2\rangle$, overlayer present; p-Si: ϵ_2, heavily doped.

Fig. 4 Parameters of an oxide film on Fe determined by simultaneous measurement of ΔR and $\Delta\rho$.

Because the less polarizable species dominates, ϵ for the rough surface region will be relatively low and will tend to appear very similar to that of an oxide overlayer. In fact, much of what passed as residual oxides in the early literature was unquestionably microscopic roughness because microscopic roughness can be positively identified only by its spectral dependence and lack of chemical reactivity.

IV. EXAMPLES

A. Cleaning and Etching

Clean, smooth, and undamaged surfaces are essential starting points for many processes, but a continuing difficulty has been the lack of techniques for unambiguously monitoring etching and cleaning in real time. The procedure discussed here is based on the dependence of the pseudodielectric function, $\langle\epsilon\rangle$, on the thickness, d, and the dielectric response, ϵ_o, of an overlayer /19/. ϵ_o and d may be average or effective values if the surface is microscopically rough or the overlayer is graded. $\langle\epsilon\rangle$ is a derived quantity calculated within the two-phase model from a measured or calculated value of ρ, and represents the dielectric response of a hypothetical homogeneous sample with a mathematically sharp interface. $\langle\epsilon\rangle$ approximates the true bulk value, ϵ, only to the extent that overlayers can be removed from the actual sample. To first order in d/λ, $\langle\epsilon\rangle$, andϵ are related by

$$\langle\epsilon\rangle = \epsilon + \frac{4\pi i d n_a}{\lambda} \frac{\epsilon(\epsilon-\epsilon_o)(\epsilon_o-\epsilon_a)}{\epsilon_o(\epsilon-\epsilon_a)} \left[\frac{\epsilon}{\epsilon_a}\sin^2\phi\right]^{1/2} \tag{6a}$$

$$\tilde{=} \epsilon + \frac{4\pi i d}{\lambda}\epsilon^{3/2}, \tag{6b}$$

where ϕ is the angle of incidence, $\epsilon_a = n_a^2$ describes the ambient, and where Eq. (6b) follows if $|\epsilon| >> |\epsilon_o| >> \epsilon_a$. Although surface characterization is usually done at a single wavelength, a spectral capability is preferred because $|\epsilon| >> |\epsilon_o|$ must be valid to guarantee uniqueness; that is, that the overlayer material is actually being removed when the data so indicate. This can be achieved for most materials only in certain wavelength ranges, for example, in the vicinity of the E_2 peak in ϵ_2 for crystalline semiconductors. Because Eq. (6b) is independent of ϵ_o, overlayer removal can be followed without having to identify the material. However, considerable information about the chemical identity of an overlayer can be obtained from its measured optical spectrum or its chemical resistance to attack by selected reagents. It is not necessary to know ϵ accurately to use this procedure.

The specific example shown in Fig. 2 illustrates the removal of the overlayer that resulted from a two-year exposure of a crystalline Si(c-Si) wafer to air /19/. A theoretical $\langle\epsilon\rangle$ trajectory, calculated by assuming that the overlayer was SiO_2, is also shown. The marks indicate thickness increments of 5Å and show that a 1Å increase in film thickness results in about a 2% decrease in the value of $\langle\epsilon_2\rangle$ at the characterization energy of 4.24 eV. Hence, the preparation method that leaves the narrowest transition region between bulk and ambient can be identified by the highest value of $\langle\epsilon_2\rangle$. The initial overlayer was 27Å thick, but 12Å could be removed with water and methanol and hence could be attributed to organic contamination. A further reduction of 12Å with HF showed this to be the true limiting thickness of the oxide. The final 3 to 4Å could only be removed with chemical polishing and preferential etching with the sequence buffered HF (BHF), bromine-methanol (BRM), BHF, NH_4OH (AMH), and BHF, indicating microscopic roughness or residual subsurface damage left over from the initial polish. Results for <111> surfaces treated with CP-4 and NaOH and for an atomically clean 7x7 reconstructed surface measured in ultrahigh vacuum are also given. The narrowest transition regions were obtained with the five-step chemical etching sequence shown. AMH was shown to improve <111> surfaces but to degrade <100> and <110> surfaces, indicating preferential etching of <111> facets on an atomic scale. Similar etching and cleaning procedures have been developed for Ge and the major III-V semiconducting compounds /20/.

B. Measurement of Dielectric Properties of Bulk Materials

"Bulk" material, as used here, means any thickness sufficient to eliminate back-surface reflection effects either by absorption or spatial separation, so that the optical properties must be determined by front-surface reflection alone. Accurate ϵ data are necessary as reference spectra and as sample and constituent data for material and thin film characterization by effective medium calculations. Ellipsometry has several advantages over reflectometry with respect to accuracy, insensitivity to light scattering by macroscopically rough surfaces, and the amount of information obtainable in a single measurement, but the single most important factor for obtaining accurate optical data (as can be inferred from the previous section) is sample preparation. Figure 2 and Eqs. (6) show that even very thin overlayers can have a large effect on apparent values of ϵ. Figure 3 shows the representative spectral dependence of overlayer-induced changes in $\langle\epsilon_2\rangle$, here measured on an atomically clean c-Si wafer that had been microscopically roughened by heating it in 10^{-8} Torr of O_2. The reference spectrum was measured on a similar sample that had been chemically cleaned as discussed above. The largest relative change occurs in the vicinity of the E_2 peak at 4.24 eV, but all regions of the spectrum are affected. Clearly, accurate ϵ data cannot be obtained unless some care is taken to remove surface overlayers and to keep the sample in an inert atmosphere to prevent overlayers from forming

during measurement. In cases where this has been done, there is very little difference between reflectance spectra for a given material whether measured directly /21/ or computed from SE data /20/.

C. Measurement of the Dielectric Properties of Thin Films

"Thin" films mean samples where back-reflection effects cannot be ignored. Such samples must be analyzed with n-phase laminar models, where $n \geqslant 3$ depending on the sharpness of the interfaces. To obtain thin-film spectra from SE data, it is necessary to solve an equation of the form

$$\rho = \rho(\epsilon;\epsilon_1,d_1;\epsilon_2,d_2,\ldots,\epsilon_a;\phi,\lambda) \tag{7}$$

where ϵ_i,d_i represent the dielectric response and thickness of the ith layer. The substrate dielectric function, ϵ, and ϕ and λ are assumed known. Even if the film is isotropic and the interfaces are sharp, at any λ there are three unknowns and only two constraints.

The most elegant solution to the problem of underdetermination is to use the reflectance-measuring capability of photometric instruments to determine the reflectance R or the reflectance change ΔR upon film growth and thereby obtain the necessary third constraint /22/. Figure 4 shows results obtained by this procedure for an oxide film on Fe /23/. The values of d provide an internal consistency check since d is a system invariant.

At present the above method is applicable only to films grown in situ because absolute values of R cannot be measured to sufficient accuracy. More generally, the additional constraint must come from varying a system parameter other than d. One possibility is ϕ, but the sensitivity is low. A more useful approach is to take advantage of interference effects, the generally widely different optical properties of ϵ and ϵ_o, and the capabilities of SE instrumentation of varying λ. Then ϵ_o can be obtained by assuming a value $<d>$ for d, solving Eq. (7) on a wavelength-by-wavelength basis for $<\epsilon_o> = \epsilon_o$, and looking for substrate- or interference-related structure in the result. The procedure can be represented formally as

$$<\epsilon_o> = \epsilon_o + (<d>-d)\frac{\partial\rho/\partial d}{\partial\rho/\partial\epsilon_o}; \tag{8}$$

only the term linear in $(<d>-d)$ contains the system parameters, and it vanishes only if $<d> = d$ in which case $<\epsilon_o> = \epsilon_o$. Sensitivity can be enhanced by differentiating the various $<\epsilon_o>$ spectra with respect to energy if necessary. If artifacts cannot be eliminated, the model for ρ is not applicable to the sample usually because the film is anisotropic or nonuniform or the interfaces are graded.

Figure 5 shows an example where the sample consists of a 5400Å thick large-grain polycrystalline Si (p-Si) film in-situ doped with phosphorus and deposited on a c-Si wafer covered with 1000Å of thermally grown oxide. A four-phase model is required, and Fig. 5 shows that the interference-related artifacts cannot be completely eliminated unless a fifth phase representing microscopic roughness at the air-film interface is also added. The total elimination of artifacts in the p-Si spectrum shows that the model accurately represents the sample. The complete spectrum of this film is given in Fig. 3.

D. Material Characterization: Long-Range Order, Doping, and Alloy Composition

Visible-near uv dielectric properties are particularly sensitive to crystalline order in the 10-100Å range owing to a corresponding sensitivity of the electronic wavefunctions. The spectral variety obtained for a series of Si samples, all consisting almost exclusively of Si atoms tetrahedrally bonded to four other Si atoms, is shown in Figs. 3 and 6. The ϵ_2 spectrum of c-Si is characterized by two sharp structures at 3.4 and 4.2 eV with the latter having a peak value of 47. For heavily doped p- (c-)Si, the lower structure is broadened substantially and both are shifted to lower energies. The shift is too small to be seen clearly in Fig. 3, but it is readily detected by Fourier or derivative methods. Changes due to the complete loss of long-range order are best represented by the amorphous Si (a-Si) spectrum in fig. 6 for the sample deposited at 571C. The sharp structures at 3.4 and 4.2 eV are completely absent, having been replaced by a broad peak near 3.7 eV. The spectrum for the a-Si sample deposited at 525C is similar in shape but is 25% lower in amplitude. This suggests by Eq. (2) that the packing is less efficient in this material, i.e., the sample is less dense. An expansion of Eq. (5) for any of the common EMTs for a two-phase composite consisting of a-Si and voids ($\epsilon_v = 1$) supports this conclusion and shows that the relative decrease in amplitude of ϵ_2 is 3/2 the relative decrease in density. Thus, the 525C sample is about 16% less dense than the 571C sample. The sample deposited at 625C shows poorly defined structure signaling the onset of polycrystallinity, but the crystallites are small. Note that all spectral dependences are quite distinct and that they differ substantially from the overlayer-distorted $<\epsilon_2>$ spectrum also shown in Fig. 3.

Optical measurements can be used to determine the composition of semiconductor alloys in several ways, the most accurate being the determination of critical point energies in optical spectra. These vary by as much as 1 eV across a given series, so in the absence of significant nonlinearity a resolution of 10 meV in the threshold energy will therefore translate into a compositional uncertainty of about 1%. Although sensitivity is generally enhanced by numeri-

cally differentiating ϵ spectra one or more times with respect to energy to bring out weak structures and to suppress baseline effects, we have recently shown that Fourier analysis can be used to advantage to optimize both noise and baseline filtering and to eliminate distortion in calculating numerical derivatives. If the critical point is isolated, the threshold energy can be obtained without having to differentiate the data at all because the slope of the phases of the Fourier coefficients plotted against coefficient index gives the critical point energy directly. Figure 7 shows such a plot for the c- and p-Si data of Fig. 3 and indicates that to within about 10 meV the introduction of $3.3 \times 10^{20} cm^{-3}$ charged impurities reduces the E_2 critical point threshold from 4.29 to 4.21 eV. Application of Fourier techniques to SE data for $GaAs_{1-x}P_x$ given elsewhere in the Proceedings /24/ illustrate further advantages of this approach.

E. Deposition and Growth: Real-Time Characterization

We cite three examples of the use of ellipsometry for real-time analysis of deposition and growth. The emphasis here is on the automatic capabilities of modern instrumentation rather than on the spectroscopic.

Figure 8 shows ellipsometrically measured (ψ,Δ) values at 5461Å for an a-Si film being deposited on a Si_3N_4 substrate /25/. The initial segment is due to the change in optical properties of the substrate upon heating to 580C. The dashed curve shows the prediction of the three-phase model assuming uniform coverage for all thicknesses. The dot-dashed curves show similar predictions but done via EMT assuming that growth occurs as hemispherical accumulations about nucleation centers. The data clearly demonstrate a nucleation growth mechanism. The spacing between centers is also obtained because the separation determines when the hemispheres will coalesce to form a continuous film. The remarkable feature of these data is that the optical measurements are sufficiently sensitive to identify the growth mechanism for thicknesses less than 2Å, far below the capabilities of any other techniques.

A second example is shown in Fig. 9, which gives the time dependence of small changes in the ellipsometric parameters measured for the growth of the (0001) face of a Cd crystal at various substrate temperatures /26/. The temperatures are represented as a supersaturation parameter σ. The ellipsometric data show oscillations that can be related to the spreading of monoatomic steps by accretion or evaporation of Cd atoms at the edges of the steps. The equilibrium condition can be determined very accurately from these data. For temperatures such that $|\Delta\sigma/\sigma_o| \lesssim 0.12$, the surfaces become rough on a larger scale. The results clearly allow conditions to be optimized during the actual growth of the material.

A final example concerns the epitaxial growth of a $Al_xGa_{1-x}As$ layer of nominal composition $x = 0.25$ by MOCVD /27/. Here, the ellipsometric data were solved as a function of time for the local refractive index $\tilde{n} = n + ik$ at 6328Å with the film thickness as a parameter. Values of $\tilde{n}$ for thickness increments of 100Å are shown in Fig. 10 after introducing the proper steady-state flow of $(CH_3)_3Al$ into the system. Instead of immediately reaching the composition $x = 0.25$, the optical data show that the film composition gradually evolved toward this value. These data were interpreted as evidence of the loss of $(CH_3)_3Al$ at other surfaces within the chamber. An increased initial flow of $(CH_3)_3Al$ was clearly required to compensate this loss in growing the composition $x = 0.25$ until the wall sites were saturated.

V. CONCLUSIONS

The fact that the old Ellipsometry Conferences have evolved into the more general theme of optical characterization is the most convincing evidence that ellipsometry is no longer perceived to be a fitting subject for study in its own right and that the emphasis has shifted to using ellipsometry to study physical systems of interest. Where do we go from here?

With respect to other visible-near uv optical techniques, it is clear that null ellipsometry, even if done at several emission lines, is no longer a competitive analytic tool but is useful only for routine measurements on elementary configurations, e.g., for determining the thicknesses of thermal oxides on single-crystal Si wafers. The amount of information obtainable at a few discrete wavelengths is severely limited no matter how clever the experimentalist. Reflectance measurements have also become much less attractive because their historic advantage -- a spectral capability -- is no longer unique. It is relatively difficult to measure reflectances to the same level of accuracy routinely attainable with complex reflectance ratios and less information is obtained at each wavelength. Although work continues to be done with null ellipsometric or reflectometric techniques, this is more a consequence of the lack of availability of commercial SE equipment. On the other hand, transmission measurements will never lose their utility for weakly absorbing samples simply because reflectance methods cannot determine absorption coefficients below 100 cm^{-1} with any degree of accuracy. Raman scattering will provide extremely useful and complementary surface information when the sensitivity problems are solved.

With respect to other spectral ranges, ellipsometry has not yet been a significant factor in either the infrared or vacuum ultraviolet partly because of the lack of good optical components but also because the information here tends to occur as individual structures relatively well localized in energy. Questions there have concerned the presence or absence of structure rather than details of the lineshapes. The situation is quite different from that of the visible-near uv, where only the single bonding-antibonding transition "line" is available and the information is contained almost entirely in its shape.

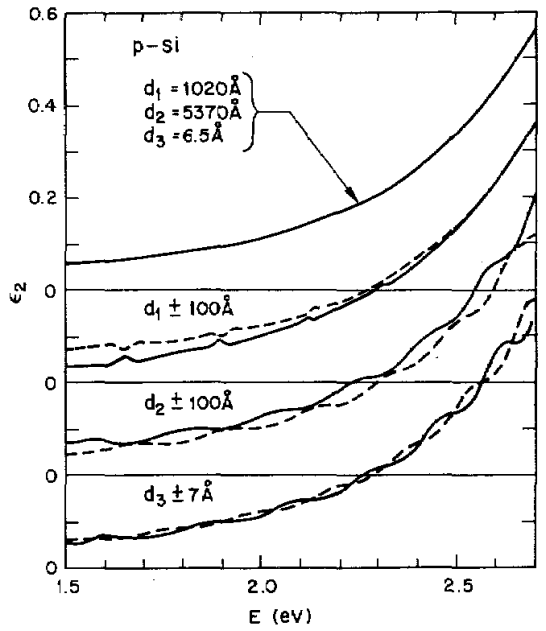

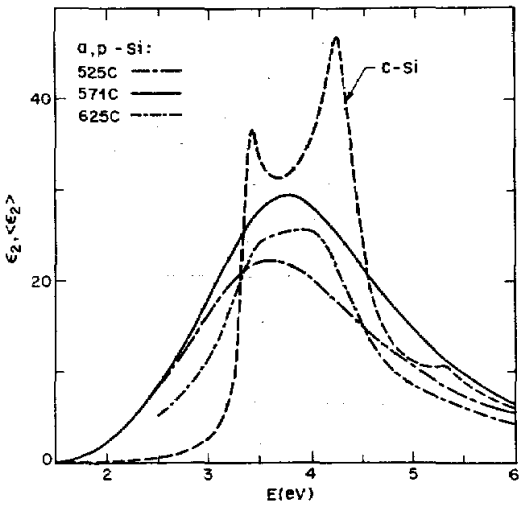

Fig. 5 $\langle\epsilon_2\rangle$ spectra for a p-Si film showing error-induced interference artifacts.

Fig. 6 ϵ_2 spectra for Si with various microstructures.

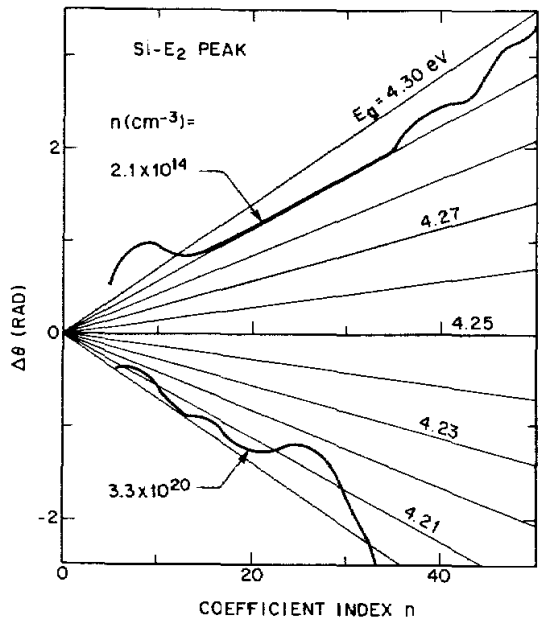

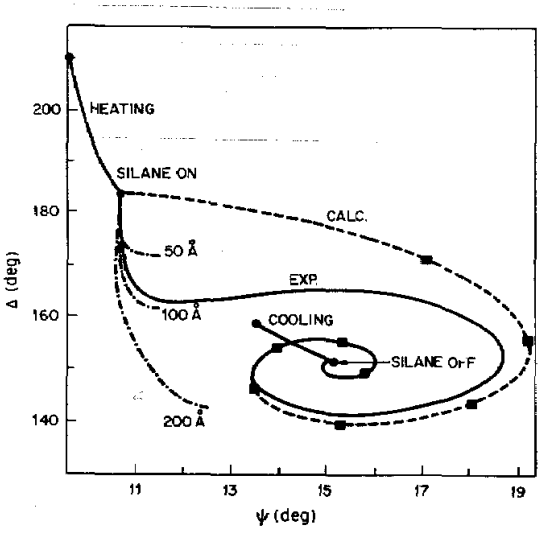

Fig. 7 Phases of the Fourier coefficients of the c- and p-Si spectra of Fig. 3 vs. coefficient index. The radial lines indicate theoretical variations for ideal critical points with the threshold energies given.

Fig. 8 Nucleation and growth of a-Si on Si_3N_4.

REFERENCES

[1] HAUGE P.S., Surf. Sci *96* (1979) 803.

[2] AZZAM R.M.A and BASHARA N.M., *Ellipsometry and Polarized Light* (North-Holland, Amsterdam, 1976).

[3] THEETEN J.B. and ASPNES D.E., Ann. Rev. Mater. Sci. *11* (1981) 97.

[4] ASPNES D.E., Thin Solid Films *89* (1982) 249.

[5] NEAL W.E.J., Appl. Surf. Sci. *2* (1979) 445.

[6] Acta Electronica *24* (1981/1982) Nos. 2 and 3.

[7] SHENG P., Phys. Rev. Lett. *45* (1980) 60.

[8] GITTLEMAN J.I. and ABELES B., Phys. Rev. B *15* (1977) 3273.

[9] GIBSON J.J. and BUHRMAN R.A., Phys. Rev. B *27* (1983) 5046.

[10] WIENER O., Abh. Math. Phys. Kl. Königl. Sächs. Ges. *32* (1912) 509.

[11] HASHIN Z. and SHTRIKMAN S., J. Appl. Phys. *33* (1962) 3125.

[12] BERGMAN D., Phys. Rev. Lett. *44* (1980) 1285.

[13] MILTON D.W., Appl. Phys. Lett. *37* (1980) 300.

[14] NIKLASSEN G.A., GRANQVIST C.G., and HUNDERI O., Appl. Opt. *20* (1981) 26.

[15] ASPNES D.E., THEETEN J.B., and HOTTIER F., Phys. Rev. B *20* (1979) 3292.

[16] STROUD D. and PAN F.P., Phys. Rev. B *17* (1978) 1502.

[17] ASPNES D.E., Phys. Rev. B *25* (1982) 1358.

[18] EGAN W.G. and ASPNES D.E., Phys. Rev. B *26* (1982) 5313.

[19] ASPNES D.E. and STUDNA A.A., SPIE Proc. *276* (1981) 227.

[20] ASPNES D.E. and STUDNA A.A., Phys. Rev. B *27* (1983) 985.

[21] DONOVAN T.M., ASHLEY E.J., and BENNETT H.E., J. Opt. Soc. Am. *53* (1963) 1403.

[22] CAHAN B.D., Surf. Sci. *56* (1976) 354.

[23] CHEN C.T. and CAHAN B.D., J. Electrochem. Soc. *129* (1982) 17.

[24] KELSO S.M. and ASPNES D.E., these Proceedings.

[25] HOTTIER F. and THEETEN J.B., J. Cryst. Growth. *48* (1980) 644.

[26] GAUCH M. and QUENTEL G., Surf. Sci. *108* (1981) 617.

[27] LAURENCE G., HOTTIER F., and HALLAIS J., Revue Phys. Appl. *16*, (1981) 579.